Computers and Electronics in Agriculture 199 (2022) 107140

Contents lists available at ScienceDirect

Computers and Electronics in Agriculture

journal homepage: www.elsevier.com/locate/compag

A low-cost integrated sensor for measuring tree diameter at breast height (DBH)

Tianyi Shao [a,b], Yonghua Qu [a,b,*], Jianqing Du [c,d]

[a] State Key Laboratory of Remote Sensing Science Jointly Sponsored by Beijing Normal University and Institute of Remote Sensing and Digital Earth of Chinese Academyof Sciences, Beijing 100875, China
[b] Beijing Engineering Research Center for Global Land Remote Sensing Products, Institute of Remote Sensing Science and Engineering, Faculty of Geographical Science, Beijing Normal University, Beijing 100875, China
[c] Beijing Yanshan Earth Critical Zone National Research Station, University of Chinese Academy of Sciences, Beijing 101408, China
[d] College of Resources and Environment, University of Chinese Academy of Sciences, Beijing 100049, China

ARTICLE INFO

Keywords:
Forestry
Diameter of breast height
Digital image processing
Laser ranging
Low-cost measurement

ABSTRACT

The measurement of tree diameter at breast height (DBH) is the basis for estimating forest timber volume, biomass, and carbon fluxes. The traditional contact methods of measuring DBH are time-consuming and labor-intensive. Thus, it is important to realize a low-cost and rapid method for measuring DBH. In this paper, a non-contact method was proposed by integrating passive (a smartphone) and active optical sensors (a laser ranger). With this device, the horizontal distance from the sensor to the tree trunk acquired by the laser ranger and the image of the target tree acquired by the smartphone were collected simultaneously. An autodetection algorithm was employed to identify the tree trunk within the image, and the diameter of the tree was then measured in combination with the horizontal distance based on the photogrammetry principle. The performance of the proposed method was validated using measuring tapes across 371 trees, the main species of which were *Italian Poplar* (*Populus euramevicana*) and *Pine (Pinus tabuliformis)* with diameters ranging from 6 to 51 cm. To investigate the factors that might affect the method, the results were further analyzed under four different conditions, i.e., varied illumination conditions, urban and natural forest conditions and different tree species with varied surface texture features. The results suggested that the measurements using the proposed device were in good agreement with those of the traditional contact method, with an absolute mean error (MAE) of 1.12 cm and RMSE of 1.55 cm. The attraction of the proposed method is that it is low-cost, portable, easy to use and sufficiently accurate. It is also expected that the proposed method can facilitate the measurement of DBH-related canopy structure parameters, such as tree volume, and other parameters, such as tree height, with little adaptation to the current version.

1. Introduction

The tree diameter at breast height (DBH) is defined as the diameter of the cross-section perpendicular to the axis of a tree trunk at 1.3 m above ground (West, 2009). The accurate measurement of DBH is critical for the estimation of tree volume and biomass (Lutz et al., 2018; Yoon et al., 2013). The established methods for measuring DBH can be divided into two types: contacting methods and non-contacting methods (Clark et al., 2000a). Traditional contact tools, such as calipers and tree girders, have been used for a long time (West, 2009). Although recognized as the most accurate method, such a contacting method is time-consuming, labor-intensive and limited by the case that is inaccessible to the target area. New contact methods have been proposed by replacing traditional tapes with electronic sensors that operated by recording the inflection of an elastic wire (Binot et al., 1995; Sun et al., 2019). Although automatic measurement is fulfilled once the contacting sensors are set up on the trees, difficulties with the inaccessibility of the target area still constrain this method's application.

Non-contacting methods have emerged in recent decades and were characterized by improved field work efficiency in forest inventory surveys. In contrast to contact methods, the non-contacting measurement methods can remotely measure the DBH at distances ranging from

* Corresponding author at: State Key Laboratory of Remote Sensing Science Jointly Sponsored by Beijing Normal University and Institute of Remote Sensing and Digital Earth of Chinese Academy of Sciences, Beijing 100875, China
E-mail addresses: sty@mail.bnu.edu.cn (T. Shao), qyh@bnu.edu.cn (Y. Qu), jqdu@ucas.ac.cn (J. Du).

https://doi.org/10.1016/j.compag.2022.107140
Received 28 December 2021; Received in revised form 12 May 2022; Accepted 11 June 2022
Available online 2 July 2022

several to tens of meters (Heinzel and Huber, 2017). From the application of the earliest film camera to charge-coupled devices (CCDs), photographic methods for measuring DBH have been widely explored (Grosenbaugh, 1963; Juujarvi et al., 1998). The basic principles for measuring DBH from either digital or analog images are similar, i.e., identifying the tree trunk in the image and constructing the ratio relationship between image and object space. A straightforward method is to set up a physical scaler (Juujarvi et al., 1998) or optical virtual scaler (such as a fixed-size laser transmitter) (Fan et al., 2020; Melkas et al., 2008; Zhang and Grift, 2012) as reference object with known size in the field of view (FOV) before photographing the tree. However, this method may be constrained by the unidentifiability of the reference object in partial scenarios (Melkas et al., 2008) and rigorous validation is required for calibrator design.

To overcome the limits of reference object-based methods, non-reference object strategies have been extensively studied in recent years. Clark et al. (2000b) empirically determined the size of the resultant image pixels by a series of images taken at varying distances. Wu et al. (2019) proposed an adaptive feature coordinate method to map the proportional relationship between the image and object space. The non-calibrator method, through the extraction of multiple features (such as coordinate and distance features) to determine the proportional relationship, is a promising method for DBH measurement, but more attention is needed to improve its automaticity and feature extraction algorithm.

Unlike the 2D image-based method of measuring DBH, the 3D profile of tree trunks reconstructed by high-density point cloud data provides the opportunity to accurately characterize the tree's structural properties and can be collected by either passive sensors, such as mono- (Marzulli et al., 2020; Mokro et al., 2018; Piermattei et al., 2019) or binocular cameras (Liu et al., 2018; Roberts et al., 2018), or active sensors, such as light detection and ranging (LiDAR).

For passive sensors, point clouds are generally fulfilled with image matching and tree trunk modeling with the help of structure-from-motion (SfM) technology (Iglhaut et al., 2019; Liu et al., 2018). The performance of this passive sensor-based method lies in the point cloud quality given the complex natural environment (Liang et al., 2014). In addition, the passive camera-based method contains a time-consuming process for data collection and processing. Marzulli et al. (2020) indicated the data quality at the plot level was determined by camera orientation, shooting mode, and photographic path. Surový et al. (2016) experimentally demonstrated that detailed modeling at the tree level required at least five cameras or viewpoints, which was time-consuming and could be aggravated by intensive postprocessing (Liang et al., 2015).

In comparison to the camera-based method, LiDAR-derived methods such as terrestrial laser scanning (TLS) (Astrup et al., 2014; Liang et al., 2018) and mobile laser scanning (MSS) (Cabo et al., 2018; Oveland et al., 2018) can directly provide point clouds from which canopy structure parameters, such as DBH, tree height and biomass (Calders et al., 2015; Maas et al., 2008). Nevertheless, the limitations of LiDAR-derived approaches remain in terms of data processing, portability and hardware costs. Specifically, Hyyppä et al. (2020) compared and discussed multiple LiDAR-driven approaches that produced acceptable accuracy, but sophisticated data processing algorithms produced higher hidden costs. Although Liang et al. (2016) indicated that the hardware costs for LiDAR have fallen, they remained a burden for forestry investigators (up to 30,000 to 80,000 euros (Liang et al., 2016)).

As the foundation for measuring DBH using 2D image-based method, reliable identification of tree trunk is essential. Fan et al. (2020) manually designated the tree trunk in field measurements; Wu et al. (2019) implemented the automatic extraction of the tree trunk utilizing a frequency-tuned algorithm; Ren et al. (2016) extracted the tree trunk boundary using an enhanced Otsu algorithm. However, the application of traditional threshold-based classification algorithms in natural environments is suffered from constraints, such as varying illumination and ambient backgrounds. Recent advancements in artificial intelligence have resulted in the application of machine learning (ML) in the identification of forest stand components. Liu et al. (2019) applied the U-net network to classify tree species in terrestrial RGB images, and the classification accuracy achieved 96.03%. Chen et al. (2018) implemented the identification of dwarf orange tree trunks based on a support vector machine to support the localization of mobile robots. However, the practical challenges associated with employing machine learning to measure basic tree properties in RGB images have yet to be addressed.

In this paper, we explore the possibility of non-contact measurement of DBH using low-cost sensors. The primary objective is to integrate a smartphone and a laser ranger to perform non-contact measurement of DBH. The secondary objective is to improve the generalizability of the proposed device by taking into account relevant impact factors. Finally, the feasibility of the DBH measurement theory is verified by accuracy evaluation and analysis with the traditional DBH contact measurement method.

2. Materials and methods

2.1. Instrument description

The developed device is designed for the non-contact measurement of standing trees in the field and consists of a smartphone (passive sensor) and a laser ranger (active sensor) that are both fixed on the tripod with a rotatable platform to ensure the level of the integrated device (Fig. 1). The smartphone is used to take a photo of the target tree, and simultaneously, the laser ranger measures the horizontal distance to the target tree. Then, the photo and horizontal distance are transmitted to the calculation module to calculate the DBH. Table 1 lists the parameters of the smartphone and laser ranger used in this paper.

2.2. Methodology

2.2.1. Overview

The focus of this study is to develop and validate a low-cost device for measuring DBH that integrates active (laser ranger) and passive (smartphone camera) optical sensors. The logical structure of the workflow consists of three parts (Fig. 2), i.e., the calibration module, the image processing module, and the calculation module. The calibration

Fig. 1. Structure of the developed device in this study.

Table 1
The main parameters of the smartphone and laser ranger*.

Type of apparatus	Model	Main parameters	Parameter Value
Smartphone	Huawei Honor 4T Pro	Photo size	3000 × 4000 pixels
		Type of Camera imaging	CMOS
		Actual focal length	5 mm
		Actual physical size of pixels [a]	0.00165 mm/pixel
		The displacement between camera and laser ranger [b]	22 cm
		Price	$ 220
Laser Ranger	Deli DL4170	Ranging pattern	Laser Ranging
		Ranging range	0.05–80 m
		Ranging accuracy	±3 mm
		Price	$ 35

* [a, b]: The calibration results were based on experimental calculations and are presented in Appendix A.

module is served as providing basic attribute information for the DBH calculation module and is divided into the camera and device calibration (Appendix A). The image processing module is used to identify the target tree through an open-source deep learning framework. Finally, the calculation module is developed by the combination of the camera imaging model and the identified tree trunk region. The basic principle of each stage is described in detail in the following sections.

2.2.2. *Image processing and accuracy evaluation*

The image processing module is designed to extract the tree trunk from RGB images and obtain the DBH in a unit of pixel, and it mainly contains two sub-processes, i.e., the determination of the target tree that multiple trees exist in the image and the identification of the tree trunk region.

In the image of a trunk, the laser spot generated by the laser ranger and the bounding rectangle of the identified region provides the opportunity to locate the target tree. To identify the spot position in the image, we firstly transform original image from RGB space into HSV (Hue, Saturation, Value) space, then empirically set global thresholds in the HSV image to extract all potential pixels (Parker, 2010), and calculate the corresponding center of gravity (Sonka et al., 2014). The extraction of the laser spot followed two assumptions:(1) the true laser spot should be near the image center; (2) the potential pixels around the true laser spot should be sparser than other pixels. The above two assumptions can be quantitatively indicated by following equation:

$$Q_a = \sqrt{k\left(\frac{n_a}{N_{point}}\right)^2 + \left(\frac{d_a}{D_{max}}\right)^2} \quad (1)$$

where N_{point} is the total potential spot pixels; n_a is the number of potential pixels for the a th center of gravity; k is the global weighting factor; D_{max} is the furthest distance from the image center; d_a is the distance between the a th potential pixel and the image center; and Q_a is the probability that the extracted ath center of gravity is the laser spot and the laser spot is identified as the smallest Q_a.

For the identification of the tree trunk region, a machine learning technique based on Baidu's open-source deep learning framework PaddlePaddle and EasyDL tool (http://ai.baidu.com/easydl) is performed to automatically identify the tree trunk. The dataset consisting of 572 images was created to train the identification model where 10% of the samples were randomly selected as the validation set. To ensure the robustness of the model, the dataset was constructed with images collected under different conditions, including illumination, measurement scenarios, tree species and image capture distances ranging from 1 to 8 m. EasyDL built a deep neural network and obtained the tree trunk classification model by combining the training set and its internal transfer learning model.

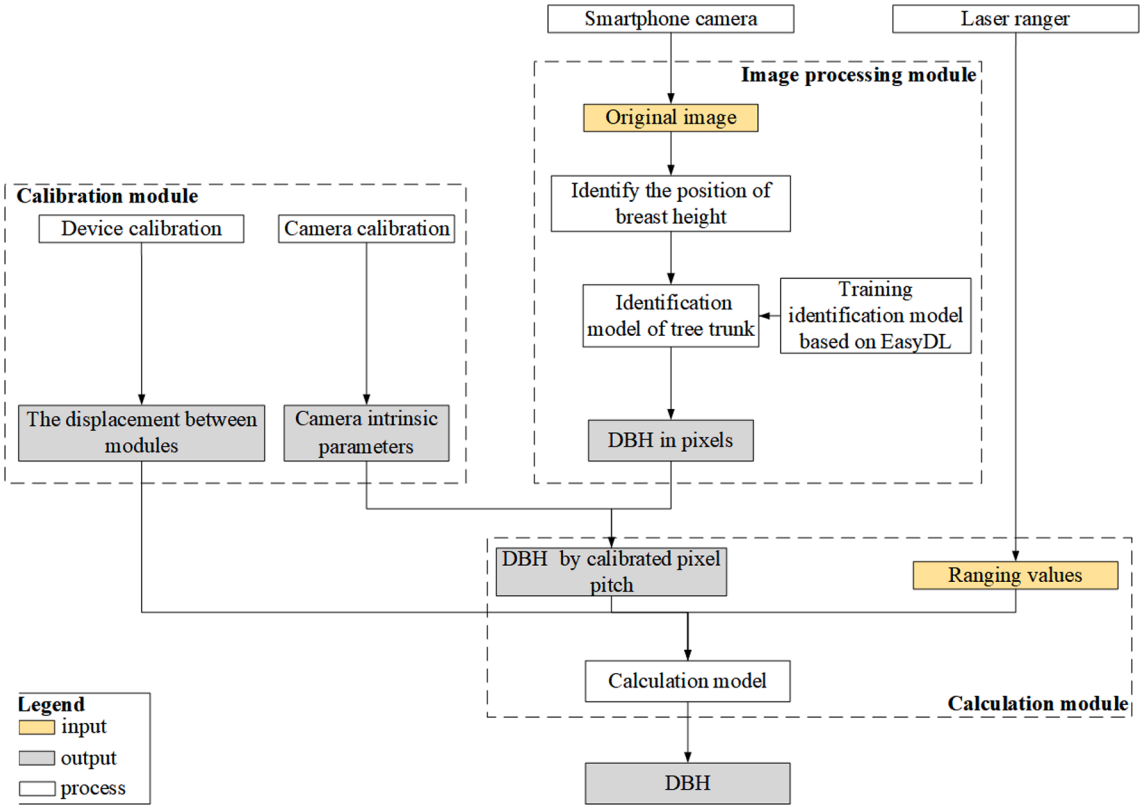

Fig. 2. Workflow of the methodology. This work is organized into three subprocesses: the calibration module, the image processing module, and the calculation module.

To assess the performance of the machine model, the precision, recall, and F-measure values were used, which were defined as follows:

$$\begin{cases} precision = \dfrac{TP}{TP + FP} \\ recall = \dfrac{TP}{TP + FN} \\ F - measure = \dfrac{2 \times precision \times recall}{precision + recall} \end{cases} \tag{2}$$

where *TP* (true positive) represents the number of samples correctly classified as trunks; *FP* (false-positive) represents the number of samples incorrectly classified as trunks; and *FN* (false negative) represents the number of trunks incorrectly classified as background. The recall and precision values can characterize the classification accuracy of tree trunks, and the F-measure value is a synthetic measurement of recall and precision assessment.

2.2.3. The DBH calculation model

The DBH can be calculated by a simple ratio equation with the help of horizontal distance and DBH in pixels (Fig. 3), and can be written as:

$$\frac{f}{d} = \frac{N \times d_x}{D_{ori}} = \frac{L_{pixel}}{D_{ori}} \tag{3}$$

where D_{ori} is the DBH, d is the horizontal distance between the device and the surface of the tree trunk, which is an initial parameter obtained by the laser ranger, f is the focal length, N is the DBH in pixels and can be estimated by a linear fitting algorithm (Appendix B) given the inclined growth of the tree in the natural environment, d_x is the calibrated pixel pitch in the image space determined by the camera calibration (Zhang, 2000), and L_{pixel} is the physical dimension of the DBH in the image.

Eq. (3) assumes that the tree trunk is rectangular and the DBH can be expressed as D_{ori} (Fig. 4). However, a better alternative is to assume the tree trunk to be cylindrical to characterize the actual situation considering the tree trunk shape characteristics (Huang et al., 2015). In this case, the actual DBH is denoted as D_{true} (Fig. 4). In addition, the distance d obtained by the laser ranger is different from the real distance d_{true}, which is defined as the distance of the device to the tree trunk center, and thus a correction method is needed. In light of this, d should be replaced by d_w, and D_{ori} should be replaced by D_w. Then, Eq. (3) can be rewritten as:

$$\frac{f}{d_w} = \frac{L_{pixel}}{D_w} \tag{4}$$

The geometric relation shown in Fig. 4 can be further represented as Eq. (5):

$$\begin{cases} \sin\alpha = \dfrac{D_{true}}{2\left(d + \dfrac{D_{true}}{2}\right)} \\ \cos\alpha = \dfrac{D_w}{D_{true}} \\ d_w = d + \dfrac{D_{true}}{2}(1 - \sin\alpha) \\ d_{true} = d + \dfrac{D_{true}}{2} \end{cases} \tag{5}$$

where d_w is the distance from the device to line AB and α is the angle between line SO and SA. Eq. (5) can be simplified and represented as Eq. (6) and the detailed DBH calculation process can be found in Appendix C.

$$D_{true}^3 + \left(d - d\frac{L_{pixel}^2}{f^2}\right)D_{true}^2 - 2d^2\frac{L_{pixel}^2}{f^2}D_{true} - \frac{L_{pixel}^2}{f^2}d^3 = 0 \tag{6}$$

2.3. Experimental data

Field data were mainly collected from two regions in China (Fig. 5a), i.e., an artificial forest (Figs. 5-b1) and an urban park (Figs. 5-b2) in Xiantao city (XT), Hubei Province, and a natural montane forest reserve (Figs. 5-b3) in Huairou District (HR), Beijing city. The montane forest (Figs. 5-c1) (about 1000 stems/ha) in HR (40°25′00″N, 116°39′37″E) was dominated by *Pine* (*Pinus tabuliformis*) forests, accompanied by tree species such as *Arborvitae* (*Platycladus orientalis*) and *Populus Canadensis* (*Populus* × *canadensis Moench*) with some shrubs in the forest, the terrain was generally undulating and uneven and finally 210 trees were measured. The artificial forest (Figs. 5-c2) (about 700 stems/ha) in XT (30°09′33″N, 113°17′38″E) was dominated by *Italian poplar* (*Populus euramevicana*) with small shrubs, the overall topography was flat with some areas of undulation, and finally 128 standing trees were measured in this area. The urban park (Figs. 5-c3) (about 600 stems/ha) in XT (30°14′14″N, 113°17′42″E) was mainly populated with *Camphor tree* (*Cinnamomum camphora (L.) Presl*), *Goldenrain tree* (*Koelreuteria paniculata*) and *Michelia chapensis* (*Michelia chapensis Dandy*), the terrain was relatively flat with no significant undulations and 37 trees were measured. In the field measurement, the tree girder and developed device were utilized synchronously to ensure the dependability of the accuracy analysis. In the case of trees in the artificial forest and urban park, the breast height was determined as the height of the tripod, which was adjusted to 1.3 m given the relatively flat terrain of the study area. For montane forests, the breast height was determined by combining the angle change of the built-in gyroscope of the smartphone. The detailed calculation procedure can be found in Appendix D.

These field measurements were conducted under four different

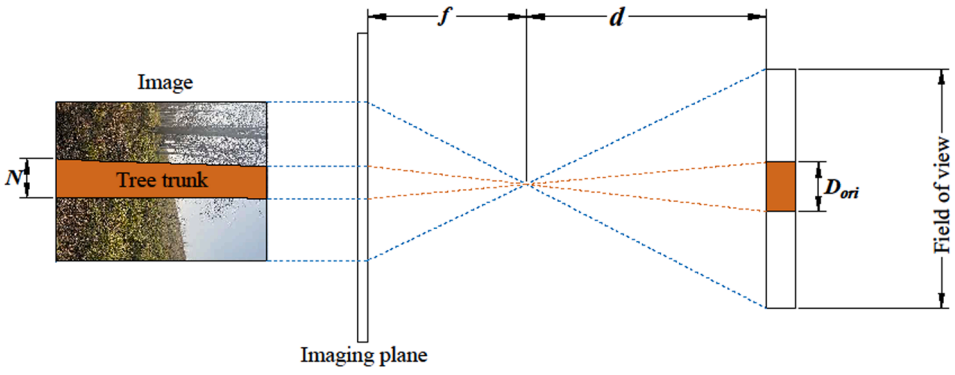

Fig. 3. The simple calculation model in top view. The DBH can be calculated by the transformation from image space (left) to object space (right) with the help of the camera focal length and range value.

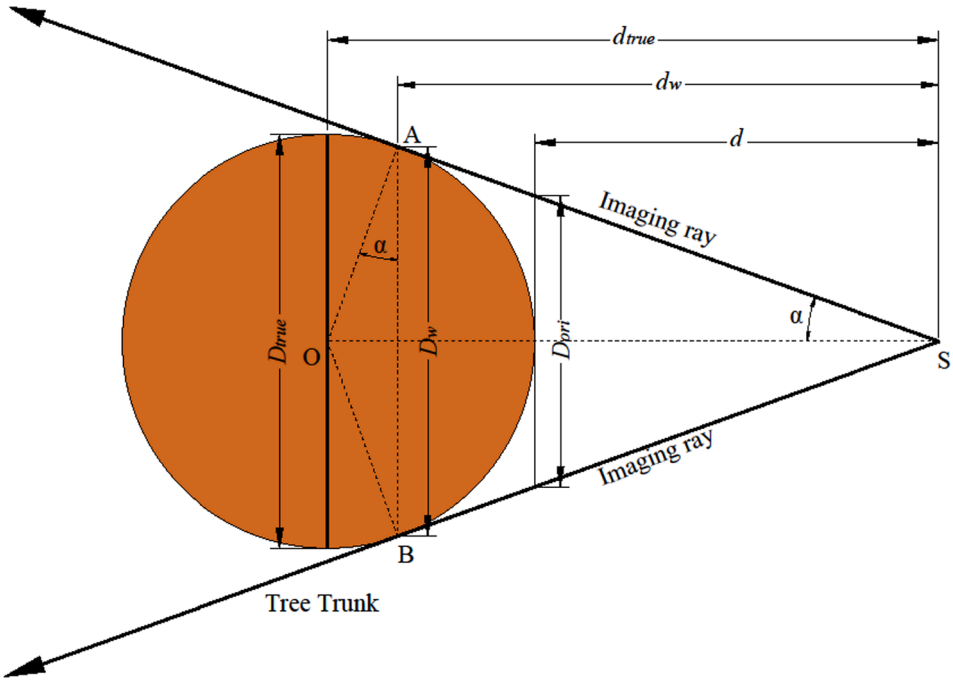

Fig. 4. The DBH calculation model. *S* is the device position, *O* is the tree trunk center, and *A*, *B* is the tangent points between the camera's optical line and the tree trunk edge.

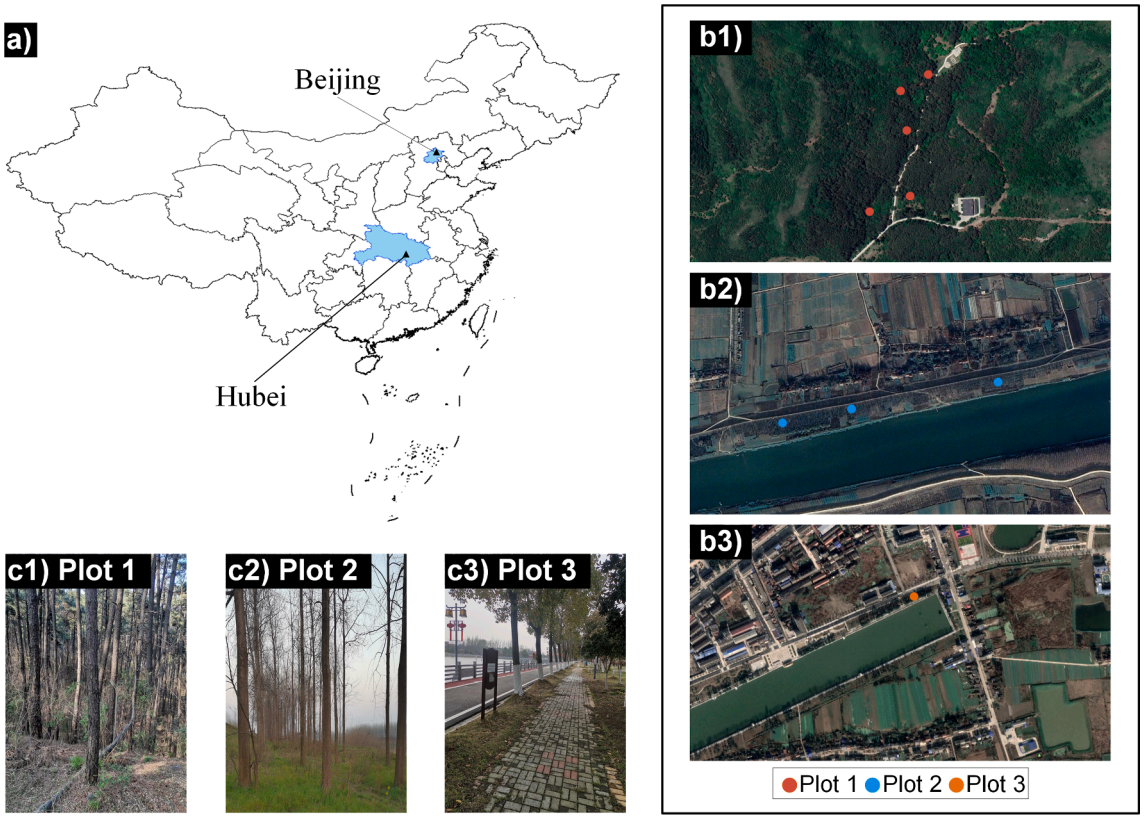

Fig. 5. The location of the study area. (a) Two regions located in China (blue polygon indicates the two provinces where the experiment was conducted). (b) The distribution of field plots in the Google Earth image. (c) Field images of different plots. (For interpretation of the references to colour in this figure legend, the reader is referred to the web version of this article.)

conditions to assess the performance of the developed device across different environments or observation configurations (E1–E4). Specifically, E1, including 21 images, represents the experiments carried out in an environment with direct light that incurs intense or nonuniform light illumination on the tree trunk surface of the target tree. E2 (containing 349 images) and E3 (49) represent the device's practicality in urban

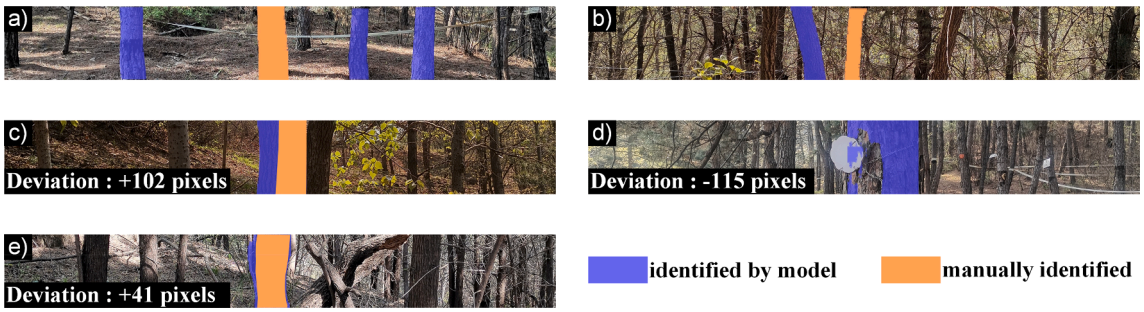

Fig. 6. Instances of tree trunks being obviously misidentified. a-b shows misidentification examples from the accuracy evaluation results of the tree trunk identification model, and c-e shows examples of DBH measurement experiments that produced significant under- or over-segmentation of trunks.

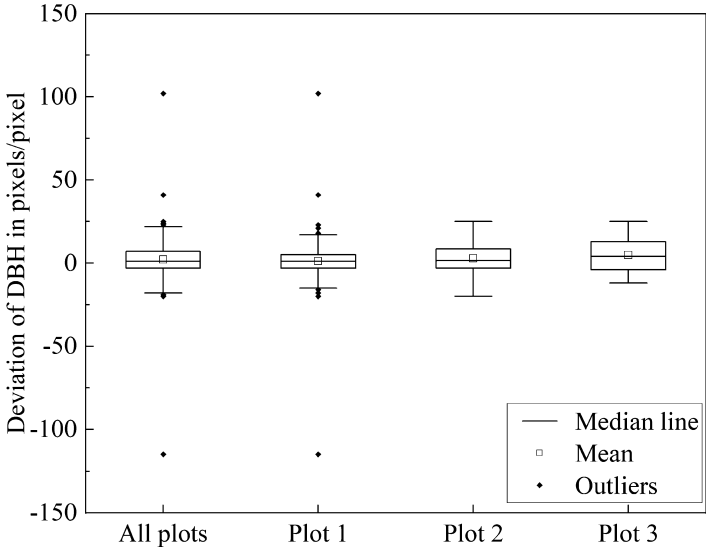

Fig. 7. The boxplot of DBH in pixels between that obtained by manual measurement from the image and that from the ML-based method.

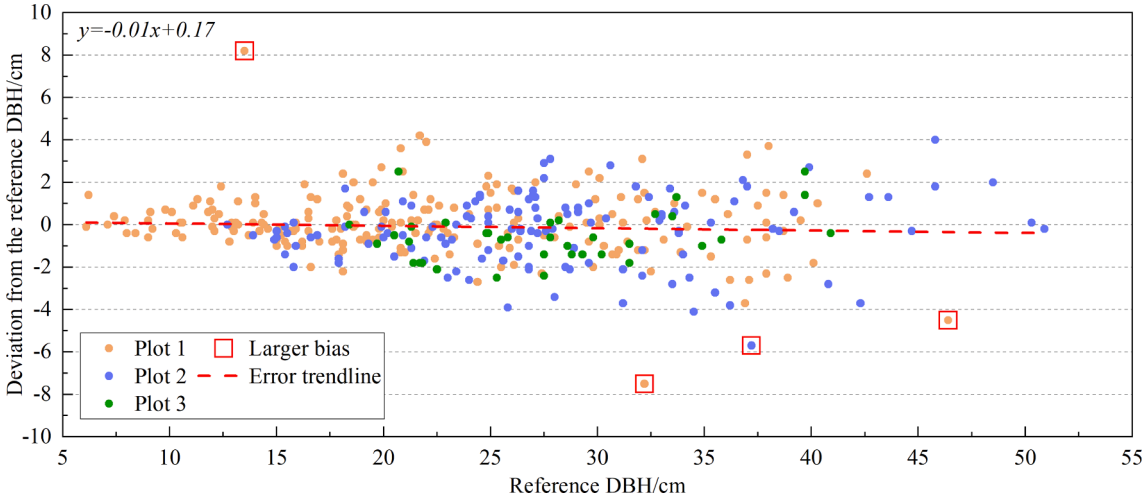

Fig. 8. The deviation between the measured DBH to the reference collected by the tree girder.

(park and roadside) and forest (simple and complex forest) scenario, respectively. An extra 26 roadside trees (E3) were measured considering the complex composition of urban areas. E4 represents the effectiveness of the device to measure tree trunks with different texture characteristics. Note that the tree numbers in E1–E4 can overlap with each other; for example, trees in urban could also be examples illuminated by direct light.

2.4. Accuracy evaluation

The reference DBH obtained by the tree girder is used to evaluate our device. We calculate the absolute mean bias (MAE), relative mean bias (reBias), root mean square error (RMSE), relative RMSE (reRMSE), and standard deviation (SD) with Eq. (7).

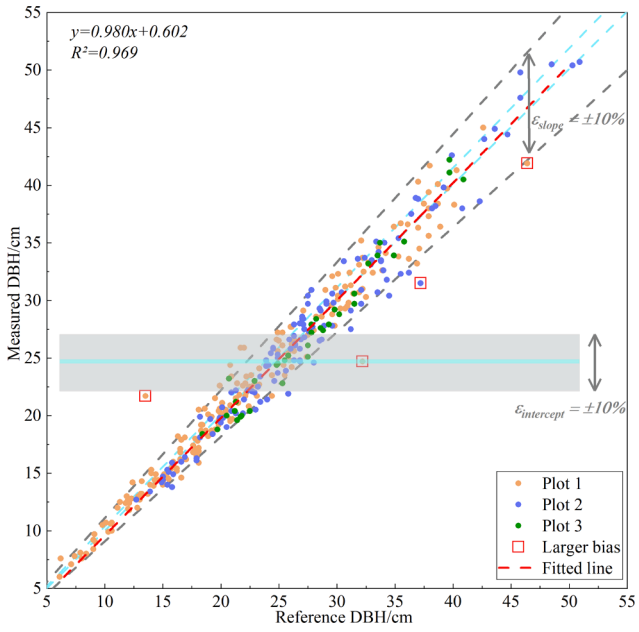

Fig. 9. Regression-based equivalence test for DBH measurements. The grey polygon and grey dashed line show the ±10% equivalence interval for the intercept and slope, respectively; the blue polygon and blue dashed line represent the 95% confidence interval for the intercept and slope, respectively. (For interpretation of the references to colour in this figure legend, the reader is referred to the web version of this article.)

$$\begin{cases} MAE = \dfrac{\sum_{i=1}^{n}|d_i - d_{ir}|}{n} \\ reBias = \dfrac{\sum_{i=1}^{n}\left(\dfrac{d_i - d_{ir}}{d_{ir}}\right)}{n} \times 100\% \\ RMSE = \sqrt{\dfrac{\sum_{i=1}^{n}(d_i - d_{ir})^2}{n}} \\ reRMSE = \sqrt{\dfrac{\sum_{i=1}^{n}\left(\dfrac{d_i - d_{ir}}{d_{ir}}\right)^2}{n}} \times 100\% \\ SD = \sqrt{\dfrac{\sum_{i=1}^{n}(|d_i - d_{ir}| - MAE)^2}{n}} \end{cases} \quad (7)$$

where n is the number of measured trees, d_i is the i th measurement, and d_{ir} is the reference value corresponding to d_i.

To compare the discrepancy between the reference DBH and measured DBH results (by our device), we used a regression-based equivalence test (Robinson et al., 2005). The test begins with the null hypothesis (H_0) of significant differences between the measured and reference value, and rejecting H_0 indicates the acceptance of the device's measurement of the DBH of the target tree. Following Robinson et al. (2005), the slope and intercept equality of the regression fitted line were tested to determine whether their two joint one-sided confidence intervals were included in the equivalence interval to decide to accept or reject the null hypothesis. In the regression-based equivalence test, the intercept component determines the difference between the measured and reference mean and represents a measure of bias; the slope component determines whether the slope of the fitted line between the measured and reference values is equal to one and represents a measure of the proportionality (de Lima et al., 2021; Yan et al., 2020). The equivalence test was conducted in R script language using the "equivalence" package (Robinson, 2016).

3. Results

3.1. Accuracy of tree trunk identification

The dataset for training the tree trunk identification model has

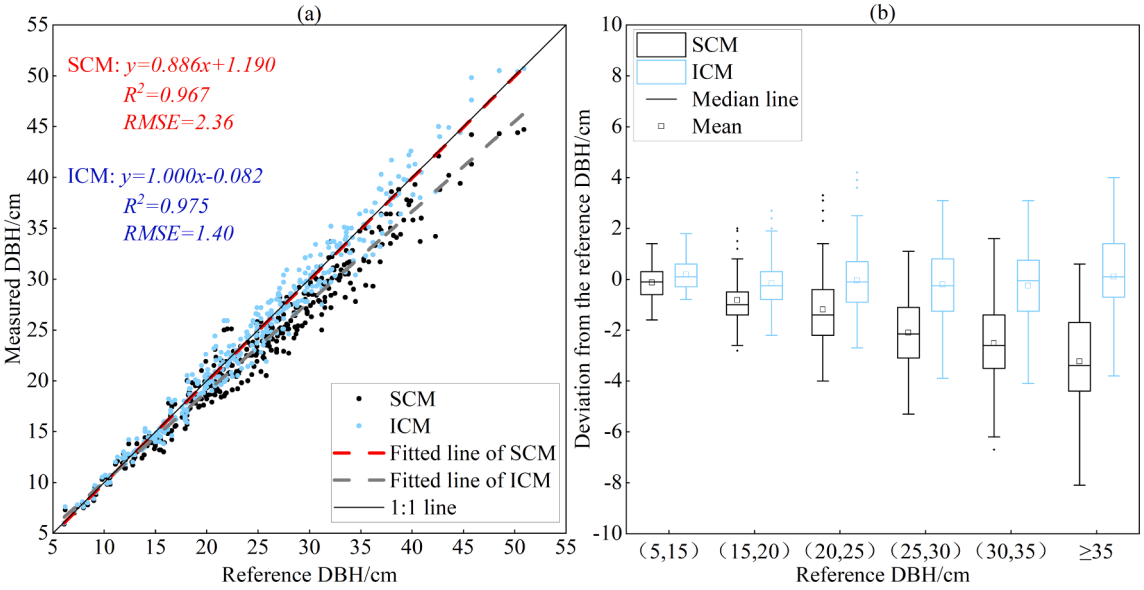

Fig. 10. The performance of the improved calculation model (ICM). (a) Comparison with simple calculation model (SCM) and ICM. (b) illustrates the grouping statistics under different calculation models.

diameters ranging from 5 to 43 cm. In the precision evaluation results for the identification model, the precision is 92.7%, recall is 100%, and F-measure is 0.96. The majority of images in the evaluation of the identification model were successfully identified, with only two exceptions of Fig. 6a and b, in which the target tree was correctly identified but the other trees were also identified as target trees.

Among the 375 samples obtained from the field work, the target trees of 4 samples were not effectively identified and further contributed to the failure of DBH measurement. To further evaluate the performance of the ML-based tree trunk identification model, we manually measured the DBH in pixels from remaining 371 images acquired in the field work as a reference. The difference between the reference and ML-based results is illustrated in Fig. 7 for different plots. There is a mean deviation of 2 pixels and an RMSE of 12 pixels for all plots. Specifically, the 25th and 75th percentiles are −3 and 7 pixels, respectively (Fig. 7), with the largest deviation of −115 pixels in Plot 1. Overall, the tree trunk is effectively-identified in most cases, while three samples produced significant deviations from the reference of + 102, −115 and + 41 pixels, respectively (Fig. 6c-e).

3.2. Statistical features of field measurement

The deviation of the measured DBH relative to the reference is shown in Fig. 8. The mean deviation for all stems from the reference amounted to −0.11 cm, with DBHs ranging from 6.1 to 50.9 cm. Only four of 371 trees had a DBH with larger bias, with the largest and smallest bias being 8.2 and −4.5 cm, respectively. There were three samples with underestimation or overestimation of DBH because of mis-segmentation of the tree trunk region, and one sample with underestimation of DBH because of incorrect operation of the device.

The accuracy indices of the measured DBH are listed in Table 2. The statistical results show that the MAE is 1.12 cm (reBias = -0.23%) and the RMSE is 1.55 cm (reRMSE = 6.64%). Fig. 9 shows the regression-based equivalence test results. The 95% confidence interval of the intercept (blue polygon) is included in the $\bar{y} \pm 10\%$ ($\bar{y}$ of the mean) equivalent interval (grey polygon), indicating the null hypothesis of dissimilarity can be rejected and measured means are equivalent to reference means. Furthermore, the 95% confidence interval for the slope (blue dashed line) lies within the $1 \pm 10\%$ equivalence interval (grey dashed line) indicating the null hypothesis of proportionality is accepted.

3.3. Performance of the developed device under different experimental conditions (E1–E4)

The error statistics between the measured DBH and reference values under different experimental conditions are presented in Table 3. Specifically, the results of dataset E1 show the measurement accuracy of the device under various lighting conditions, with MAE = 0.95 cm and RMSE = 1.30 cm. In the overall error statistics for artificial forest of simple stands and montane forest of complex stands included in dataset E2, no significant differences were observed between the measured values and the reference (MAE = 1.12 cm, RMSE = 1.57 cm). For E3, all trees could be measured effectively in 49 trees in both experimental conditions of urban park and street trees. Among the experiments involved six tree species with different texture features (E4), the device can effectively identify and measure the majority of the trunks, while one sample resulted in significant under-segmentation of the target tree due to the high similarity of the texture features to the background.

3.4. Performance of the DBH calculation model

An improved DBH calculation model in this paper was applied to correct the misestimation of DBH in Eq. (3). The performances of using the improved calculation model and the simple calculation model are shown in Fig. 10. For comparison, 4 samples with larger bias in the dataset were excluded (Fig. 8). The statistical results show a considerable reduction of bias (Fig. 10a), from −1.61 to −0.08 cm (RMSE from 2.36 to 1.40 cm). Specifically, the calculation model allows for the systematic improvement of DBH measuring accuracy for different stem diameters (Fig. 10b), especially for large-diameter trees with DBH>35 cm.

4. Discussion

4.1. DBH measurement performance

Overall, the integrated active and passive optical sensors in this study were able to provide the result of small error statistics (e.g., MAE = 1.12 cm, RMSE = 1.55 cm). For comparison purposes, we collected previous papers using SfM, LiDAR, and other similar methods and compared the statistical results with each other (Table 4). Although it is difficult to make a direct comparison with previous studies because of incompatible elements that may impact the statistical results, the comparisons in Table 4 offer an overview of their performance.

Apparently, among all the methods, the cost of our device is minimum. The measurement accuracy in this study is maintained at roughly the same level as previous approaches, although there are differences in forest stand conditions. Specifically, our method is comparable to the measurement accuracy of HMLS and TOF camera, while TLS provides the smallest bias (Table 4).

4.2. Impact of experimental background and measurement mode

The effect of the experimental background on the DBH measurement is shown in the estimation of DBH in pixels. This parameter directly determines the transformation of image space to object space and further influences DBH. For simple and fixed experimental backgrounds, traditional image processing algorithms have a robust performance (Huang et al., 2015; Juujarvi et al., 1998; Melkas et al., 2008; Wu et al., 2019) attributed to the distinguishability of tree trunks.

For tree trunk identification in natural scenes, the variable experimental backgrounds may constrain the generalization of the identification model. However, in combination with the extracted laser spot and the bounding rectangle as a priori knowledge to locate the target tree, the robustness of the identification model can be further improved. The statistical results (Fig. 7) support their validity that DBH in pixels is not significantly biased by model misclassification (i.e., other trees are identified as the target tree). Nevertheless, there are still cases that the target tree is not correctly segmented because of the overlapping of trees

Table 2
The accuracy indices of DBH measured by the developed device*.

	N	MAE (cm)	reBias (%)	RMSE (cm)	reRMSE (%)	Min/max error (cm)	SD (cm)
Plot 1	206	1.04	0.84	1.52	7.37	0.0/8.2	1.12
Plot 2	128	1.28	−1.17	1.70	5.71	0/-5.7	1.10
Plot 3	37	1.06	−2.34	1.29	4.99	0.0/±2.5	0.74
All stems	371	1.12	−0.23	1.55	6.64	0.0/8.2	1.07

* MAE: absolute mean error; reBias: relative mean error; RMSE: root mean square error; reRMSE: relative RMSE. Min/max: minimum error/ maximum error; SD: standard deviation.

Table 3
Accuracy of DBH measured under different measurement conditions.

	Dominant Species	Range	N	MAE (cm)	reBias (%)	RMSE (cm)	reRMSE (%)	SD (cm)
E1	*Italian Poplar, Goldenrain tree, Camphor tree, Cypress*	(14, 42)	21	0.95	−0.63	1.30	4.52	0.91
E2	*Italian Poplar, Cypress, Arborvitae, Populus Canadensis, Pine*	(6, 51)	349	1.12	0.05	1.57	6.73	1.10
E3	*Italian Poplar, Pine, Goldenrain tree*	(14, 41)	49	0.95	−1.51	1.18	4.65	0.57
E4	*Italian Poplar*	(13, 51)	128	1.27	−1.37	1.66	5.79	1.10
	Camphor tree	(21, 41)	21	1.15	−1.06	1.33	4.65	0.68
	Goldenrain tree	(19, 36)	16	0.89	−3.74	1.57	6.31	0.66
	Arborvitae	(6, 38)	18	0.78	3.51	1.02	7.95	0.67
	Populus Canadensis	(18, 41)	13	1.36	−2.59	1.72	6.38	1.05
	Pine	(7, 47)	175	1.04	0.88	1.55	7.42	1.15

Table 4
Accuracy comparison of DBH measurement by different methods*.

Method [a]	Bias (cm)	reBias (%)	RMSE (cm)	reRMSE (%)	Range [b]	N [c]	Forest type [d]	Main species [e]	Price [f] ($)	Reference and source
Ours	−0.11	−0.23	1.55	6.64	(6, 51)	371	AF/MF/UAF	MS1	255	This study
HMLS	−0.39	−1.40	0.90	3.50	(5,58)	68	NBF	MS2	1500	(Hyyppä et al., 2020) Table 1, Table 2 & Table 7
TLS	0.04	0.20	1.67	7.20	(5.65)	407	NBF	MS3	>1500	(Kankare et al., 2015) Fig. 5 & Table 2
SfM	−0.77	−3.77	1.62	7.73	(4,64)	140	UAF	MS4	>450	(Roberts et al., 2019) Table 2
TOF camera	0.33	1.78	1.26	6.39	(5,40)	193	AF	MS5	600	(Fan et al., 2018) Table 1 & Table 3

*The data were digitized and recompiled from the figures in the cited works, and there might be a slight bias to the original results. In addition, owing to the inability to control the consistency of forest stand conditions in different papers, our comparison can only provide some reference, and detailed results need to be carried out in more rigorous experiments. [a]: HMLS: Hand-held Mobile Laser Scanning, TLS: Terrestrial Laser Scanning, SfM: Structure from Motion, TOF camera: Time of Flight camera. [b]: Distribution range of measured values. [c]: The number of trees measured. [d]: AF: artificial forest, MF: montane Forest, UAF: urban artificial forest, NBF: norwegian boreal forest. [e]: MS1: *Italian poplar, Camphor tree, Goldenrain tree, Arborvitae and Populus Canadensis, Pine*; MS2: *Pine, Spruces, Birches*; MS3: *Scots pine, Norway spruce*; MS4: *Loblolly pine, Virginia oak, Laurel oak*; MS5: *Ginkgo, Elm*. [f]: The prices of the devices used in the cited study, which have been converted to USD after exchange rate calculations.

with similar texture features (Fig. 6c) and the existence of interferences (Fig. 6d), which puts forward higher requirements for the image segmentation algorithm since manual segmentation is also difficult in this case.

Apart from the performance of the identification model, factors related to the data collection approach also play an important role in the DBH measurement. The premise for applying an image-based method is the acquisition of complete tree trunk (Fan et al., 2020, 2018) because of its lack of the ability to penetrate the gaps in leaves or fine branches as LiDAR (Liang et al., 2014). In this study, the optimal observation orientation was determined by the operator based on practical site-level conditions, which was similar to the TLS to improve the detection rates by multistand scanning (Liang et al., 2016). Fortunately, this yielded positive results that there was no application failure attributed to interference occlusion, although the performance might vary from case to case for different forest stands.

The systematic error of DBH calculation can be mainly attributed to the tree inclination angle and ranging error on the transformation between object and image space. In the 2D image-based mode, the ranging error is equal to half of the DBH so that the ranging error increases as the stem diameter becomes larger. The deviation of the intersection line D_w (Fig. 4) formed by the camera's divergence view and tree trunk from the true DBH (D_{true}) is greater as stem diameter increases. Overall, the results (Fig. 10) show the necessity of taking camera imaging patterns and ranging errors into account when measuring DBH from a 2D perspective.

4.3. Further research

This paper developed a DBH measurement device by integrating active and passive optical sensors in field data collection. Nevertheless, it should be noted that some aspects have been simplified or not considered while more research work is still required to improve the operability and applicability of the device.

In this study, a manual leveling procedure was used to obtain the horizontal distance and vertical projection geometry, which might introduce random errors of manual operation. From the view of combining multi-source data, quantitative estimation of the device pose may provide a reasonable solution to minimize random errors, such as integrating additional sensors of inertial measurement unit (Pierzchała et al., 2018) and combining simultaneous localization and mapping for optimization (Fan et al., 2018; Hyyppä et al., 2017). All the above multi-source data can be applied to broaden the usability of the device in terms of applicable scenarios and device operability.

Although the inclination angle of the target tree in the two-dimensional view is quantitatively estimated in this paper (Appendix B), the projection results may vary significantly with the change of observation view. In addition, the tree trunk shape is always irregular from the cross-sectional perspective (Clark et al., 2000a), resulting in discrepancies in DBH measurements from various viewpoints. The potential options in further field measurements are the 3D reconstruction of significantly inclined trees from multiple viewpoints (Hapca et al., 2007) for significantly inclined trees and to develop high-precision solution models accounting for multiple factors.

5. Conclusions

This paper developed a non-contact device to measure DBH by integrating active (laser ranger) and passive (smartphone) optical sensors. With such a device, automatic measurement of DBH can be conducted with less subjective manual intervention compared to traditional methods using tree girders. In our method, the laser ranger was adjusted to the horizontal to determine the ratio relationship between the image and object space, and the image was employed to determine the DBH in pixels based on an ML-based identification algorithm. The results

confirm that the combined consumer level devices can achieve acceptable precision of DBH with a noncontact mode. The statistical results of the measured DBH showed agreement with the reference value of the tree girder among the five accuracy evaluation indicators, with MAE, reBias, RMSE, reRMSE and SD of 1.12 cm, −0.23%, 1.55 cm, 6.64% and 1.07 cm respectively. The success of the DBH measurement was attributed to the robust image identification algorithm and developed calculation model. Our method's advantages are in terms of low cost, simpler system structure and less expertise required.

In future studies, a more rigorous integrated structure of active–passive remote sensing should be explored to minimize the impacts of improper operation. Meanwhile, more forest structural parameters, such as tree height, volume and biomass, should be extracted to fulfill the demands of forest surveying work.

Declaration of Competing Interest

The authors declare that they have no known competing financial interests or personal relationships that could have appeared to influence the work reported in this paper.

Acknowledgements

This work was supported in part by the National Natural Science Foundation of China (NO. 42192581). We thank the graduate student Yaowei Feng for his help in data collection in HR region. We sincerely appreciate researcher Min Zhang from Beijing Yanshan Earth Critical Zone National Research Station in University of Chinese Academy of Sciences for providing support to the field experiment.

Appendix A. Supplementary material

Supplementary data to this article can be found online at https://doi.org/10.1016/j.compag.2022.107140.

References

Astrup, R., Ducey, M.J., Granhus, A., Ritter, T., von Lüpke, N., 2014. Approaches for estimating stand-level volume using terrestrial laser scanning in a single-scan mode. Can. J. For. Res. 44 (6), 666–676. https://doi.org/10.1139/cjfr-2013-0535.

Binot, J.-M., Pothier, D., Lebel, J., 1995. Comparison of relative accuracy and time requirement between the caliper, the diameter tape and an electronic tree measuring fork. For. Chron. 71 (2), 197–200. https://doi.org/10.5558/tfc71197-2.

Cabo, C., Del Pozo, S., Rodríguez-Gonzálvez, P., Ordóñez, C., González-Aguilera, D., 2018. Comparing terrestrial laser scanning (TLS) and wearable laser scanning (WLS) for individual tree modeling at plot level. Remote Sens. 10 (4), 540. https://doi.org/10.3390/rs10040540.

Calders, K., Newnham, G., Burt, A., Murphy, S., Raumonen, P., Herold, M., Culvenor, D., Avitabile, V., Disney, M., Armston, J., Kaasalainen, M., McMahon, S., 2015. Nondestructive estimates of above-ground biomass using terrestrial laser scanning. Methods Ecol. Evol. 6 (2), 198–208. https://doi.org/10.1111/2041-210X.12301.

Chen, X., Wang, S., Zhang, B., Luo, L., 2018. Multi-feature fusion tree trunk detection and orchard mobile robot localization using camera/ultrasonic sensors. Comput. Electron. Agric. 147, 91–108. https://doi.org/10.1016/j.compag.2018.02.009.

Clark, N.A., Wynne, R.H., Schmoldt, D.L., 2000a. A review of past research on dendrometers. For. Sci. 46, 570–576. https://doi.org/10.1093/forestscience/46.4.570.

Clark, N.A., Wynne, R.H., Schmoldt, D.L., Winn, M., 2000b. An assessment of the utility of a non-metric digital camera for measuring standing trees. Comput. Electron. Agric. 28 (2), 151–169. https://doi.org/10.1016/S0168-1699(00)00125-3.

de Lima, R.S., Lang, M., Burnside, N.G., Peciña, M.V., Arumäe, T., Laarmann, D., Ward, R.D., Vain, A., Sepp, K., 2021. An Evaluation of the Effects of UAS Flight Parameters on Digital Aerial Photogrammetry Processing and Dense-Cloud Production Quality in a Scots Pine Forest. Remote Sens. 13, 1121. https://doi.org/10.3390/rs13061121.

Fan, G., Feng, W., Chen, F., Chen, D., Dong, Y., Wang, Z., 2020. Measurement of volume and accuracy analysis of standing trees using Forest Survey Intelligent Dendrometer. Comput. Electron. Agric. 169, 105211. https://doi.org/10.1016/j.compag.2020.105211.

Fan, Y., Feng, Z., Mannan, A., Khan, T., Shen, C., Saeed, S., 2018. Estimating tree position, diameter at breast height, and tree height in real-time using a mobile phone with RGB-D SLAM. Remote Sens. 10 (11), 1845. https://doi.org/10.3390/rs10111845.

Grosenbaugh, L.R., 1963. Optical dendrometers for out-of-reach diameters: a conspectus and some new theory. For. Sci. 9, a0001–a47. https://doi.org/10.1093/forestscience/9.s1.a0001.

Hapca, A.I., Mothe, F., Leban, J.-M., 2007. A digital photographic method for 3D reconstruction of standing tree shapeMesure de la forme des arbres sur pied par photogrammétrie. Ann. For. Sci. 64 (6), 631–637. https://doi.org/10.1051/forest:2007041.

Heinzel, J., Huber, M.O., 2017. Tree stem diameter estimation from volumetric TLS image data. Remote Sens. 9, 1–11. https://doi.org/10.3390/rs9060614.

Huang, X.D., Feng, Z., Xie, M., Chen, J., Liu, J., 2015. Developing and accuracy analysis of portable device for automatically measuring diameter at breast height and tree height. Trans. Chinese Soc. Agric. Eng. (in Chinese) 31, 92–99. https://doi.org/10.11975/j.issn.1002-6819.2015.18.014.

Hyyppä, E., Yu, X., Kaartinen, H., Hakala, T., Kukko, A., Vastaranta, M., Hyyppä, J., 2020. Comparison of backpack, handheld, under-canopy UAV, and above-canopy UAV laser scanning for field reference data collection in boreal forests. Remote Sens 12 (20), 3327. https://doi.org/10.3390/rs12203327.

Hyyppä, J., Virtanen, J.-P., Jaakkola, A., Yu, X., Hyyppä, H., Liang, X., 2017. Feasibility of Google Tango and Kinect for Crowdsourcing Forestry Information. Forests 9, 6. https://doi.org/10.3390/f9010006.

Iglhaut, J., Cabo, C., Puliti, S., Piermattei, L., O'Connor, J., Rosette, J., 2019. Structure from Motion Photogrammetry in Forestry: a Review. Curr. For. Reports 5 (3), 155–168. https://doi.org/10.1007/s40725-019-00094-3.

Juujarvi, J., Heikkonen, J., Brandt, S.S., Lampinen, J., 1998. Digital Image Based Tree Measurement for Forest Inventory, in: Casasent, D.P. (Ed.), Intelligent Robots and Computer Vision XVII: Algorithms, Techniques, and Active Vision. Bellingham, WA, USA, pp. 114–123. https://doi.org/10.1117/12.325754.

Kankare, V., Liang, X., Vastaranta, M., Yu, X., Holopainen, M., Hyyppä, J., 2015. Diameter distribution estimation with laser scanning based multisource single tree inventory. ISPRS J. Photogramm. Remote Sens. 108, 161–171. https://doi.org/10.1016/j.isprsjprs.2015.07.007.

Liang, X., Hyyppä, J., Kaartinen, H., Lehtomäki, M., Pyörälä, J., Pfeifer, N., Holopainen, M., Brolly, G., Francesco, P., Hackenberg, J., Huang, H., Jo, H.W., Katoh, M., Liu, L., Mokroš, M., Morel, J., Olofsson, K., Poveda-Lopez, J., Trochta, J., Wang, D., Wang, J., Xi, Z., Yang, B., Zheng, G., Kankare, V., Luoma, V., Yu, X., Chen, L., Vastaranta, M., Saarinen, N., Wang, Y., 2018. International benchmarking of terrestrial laser scanning approaches for forest inventories. ISPRS J. Photogramm. Remote Sens. 144, 137–179. https://doi.org/10.1016/j.isprsjprs.2018.06.021.

Liang, X., Jaakkola, A., Wang, Y., Hyyppä, J., Honkavaara, E., Liu, J., Kaartinen, H., 2014. The use of a hand-held camera for individual tree 3D mapping in forest sample plots. Remote Sens. 6, 6587–6603. https://doi.org/10.3390/rs6076587.

Liang, X., Kankare, V., Hyyppä, J., Wang, Y., Kukko, A., Haggrén, H., Yu, X., Kaartinen, H., Jaakkola, A., Guan, F., Holopainen, M., Vastaranta, M., 2016. Terrestrial laser scanning in forest inventories. ISPRS J. Photogramm. Remote Sens. 115, 63–77. https://doi.org/10.1016/j.isprsjprs.2016.01.006.

Liang, X., Wang, Y., Jaakkola, A., Kukko, A., Kaartinen, H., Hyyppa, J., Honkavaara, E., Liu, J., 2015. Forest data collection using terrestrial image-based point clouds from a handheld camera compared to terrestrial and personal laser scanning. IEEE Trans. Geosci. Remote Sens. 53 (9), 5117–5132. https://doi.org/10.1109/TGRS.2015.2417316.

Liu, J., Feng, Z., Yang, L., Mannan, A., Khan, T.U., Zhao, Z., Cheng, Z., 2018. Extraction of sample plot parameters from 3D point cloud reconstruction based on combined RTK and CCD continuous photography. Remote Sens. 10, 1299. https://doi.org/10.3390/RS10081299.

Liu, J., Wang, X., Wang, T., 2019. Classification of tree species and stock volume estimation in ground forest images using Deep Learning. Comput. Electron. Agric. 166, 105012. https://doi.org/10.1016/j.compag.2019.105012.

Lutz, J.A., Furniss, T.J., Johnson, D.J., Davies, S.J., Allen, D., Alonso, A., Anderson-Teixeira, K.J., Andrade, A., Baltzer, J., Becker, K.M.L., Blomdahl, E.M., Bourg, N.A., Bunyavejchewin, S., Burslem, D.F.R.P., Cansler, C.A., Cao, K.e., Cao, M., Cárdenas, D., Chang, L.-W., Chao, K.-J., Chao, W.-C., Chiang, J.-M., Chu, C., Chuyong, G.B., Clay, K., Condit, R., Cordell, S., Dattaraja, H.S., Duque, A., Ewango, C.E.N., Fischer, G.A., Fletcher, C., Freund, J.A., Giardina, C., Germain, S.J., Gilbert, G.S., Hao, Z., Hart, T., Hau, B.C.H., He, F., Hector, A., Howe, R.W., Hsieh, C.-F., Hu, Y.-H., Hubbell, S.P., Inman-Narahari, F.M., Itoh, A., Janík, D., Kassim, A.R., Kenfack, D., Korte, L., Král, K., Larson, A.J., Li, YiDe, Lin, Y., Liu, S., Lum, S., Ma, K., Makana, J.-R., Malhi, Y., McMahon, S.M., McShea, W.J., Memiaghe, H.R., Mi, X., Morecroft, M., Musili, P.M., Myers, J.A., Novotny, V., de Oliveira, A., Ong, P., Orwig, D.A., Ostertag, R., Parker, G.G., Patankar, R., Phillips, P.R., Reynolds, G., Sack, L., Song, G.-Z., Su, S.-H., Sukumar, R., Sun, I.-F., Suresh, H.S., Swanson, M.E., Tan, S., Thomas, D.W., Thompson, J., Uriarte, M., Valencia, R., Vicentini, A., Vrška, T., Wang, X., Weiblen, G.D., Wolf, A., Wu, S.-H., Xu, H., Yamakura, T., Yap, S., Zimmerman, J.K., Kerkhoff, A., 2018. Global importance of large-diameter trees. Glob. Ecol. Biogeogr. 27 (7), 849–864. https://doi.org/10.1111/geb.12747.

Maas, H.-G., Bienert, A., Scheller, S., Keane, E., 2008. Automatic forest inventory parameter determination from terrestrial laser scanner data. Int. J. Remote Sens. 29 (5), 1579–1593. https://doi.org/10.1080/01431160701736406.

Marzulli, M.I., Raumonen, P., Greco, R., Persia, M., Tartarino, P., 2020. Estimating tree stem diameters and volume from smartphone photogrammetric point clouds. Forestry 93, 411–429. https://doi.org/10.1093/forestry/cpz067.

Melkas, T., Vastaranta, M., Holopainen, M., 2008. Accuracy and Efficiency of the Laser-camera, in: Proceedings of SilviLaser 2008, 8th International Conference on LiDAR Applications in Forest Assessment and Inventory. Edinburgh,UK, pp. 315–324.

Mokro, M., Liang, X., Surový, P., Valent, P., Čerňava, J., Chudý, F., Tunák, D., Saloň, I., Merganič, J., 2018. Evaluation of close-Range photogrammetry image collection

methods for estimating tree diameters. ISPRS Int. J. Geo-Information 7, 93. https://doi.org/10.3390/ijgi7030093.
Oveland, I., Hauglin, M., Giannetti, F., Kjørsvik, N.S., Gobakken, T., 2018. Comparing three different ground based laser scanning methods for tree stem detection. Remote Sens. 10, 1–17. https://doi.org/10.3390/rs10040538.
Parker, J.R., 2010. Algorithm for Image Processing and Computer Vision. John Wiley & Sons, Indianapolis, Ind.
Piermattei, L., Karel, W., Wang, D., Wieser, M., Mokroš, M., Surový, P., Koreň, M., Tomaštík, J., Pfeifer, N., Hollaus, M., 2019. Terrestrial Structure from Motion Photogrammetry for Deriving Forest Inventory Data. Remote Sens. 11, 950. https://doi.org/10.3390/rs11080950.
Pierzchała, M., Giguère, P., Astrup, R., 2018. Mapping forests using an unmanned ground vehicle with 3D LiDAR and graph-SLAM. Comput. Electron. Agric. 145, 217–225. https://doi.org/10.1016/j.compag.2017.12.034.
Ren, H., Zhou, Y., Zhu, M., 2016. Tree image segmentation based on an improved two-dimensional otsu algorithm. Int. J. Hybrid Inf. Technol. 9 (9), 199–210.
Roberts, J., Koeser, A., Abd-Elrahman, A., Wilkinson, B., Hansen, G., Landry, S., Perez, A., 2019. Mobile terrestrial photogrammetry for street tree mapping and measurements. Forests 10, 1–16. https://doi.org/10.3390/f10080701.
Roberts, J.W., Koeser, A.K., Abd-Elrahman, A.H., Hansen, G., Landry, S.M., Wilkinson, B. E., 2018. Terrestrial photogrammetric stem mensuration for street trees. Urban For. Urban Green. 35, 66–71. https://doi.org/10.1016/j.ufug.2018.07.016.
Robinson, A.P., 2016. Provides Tests and Graphics for Assessing Tests of equivalence. R package version 0.7.2. https://CRAN.R-project.org/package=equivalence, accessed: March 21, 2022.
Robinson, A.P., Duursma, R.A., Marshall, J.D., 2005. A regression-based equivalence test for model validation: shifting the burden of proof. Tree Physiol. 25 (7), 903–913. https://doi.org/10.1093/treephys/25.7.903.
Sonka, M., Hlavac, V., Boyle, R., 2014. Image Processing, Analysis, and Machine Vision. Cengage Learning, Toronto.
Sun, L., Fang, L., Weng, Y., Zheng, S., 2019. An integrated method for coding trees, measuring tree diameter, and estimating tree positions. Sensors 20, 144. https://doi.org/10.3390/s20010144.
Surový, P., Yoshimoto, A., Panagiotidis, D., 2016. Accuracy of reconstruction of the tree stem surface using terrestrial close-range photogrammetry. Remote Sens. 8 (2), 123. https://doi.org/10.3390/rs8020123.
West, P.W., 2009. In: Tree and Forest Measurement. Springer Berlin Heidelberg, Berlin, Heidelberg.
Wu, X., Zhou, S., Xu, A., Chen, B., 2019. Passive measurement method of tree diameter at breast height using a smartphone. Comput. Electron. Agric. 163, 104875. https://doi.org/10.1016/j.compag.2019.104875.
Yan, W.Y., van Ewijk, K., Treitz, P., Shaker, A., 2020. Effects of radiometric correction on cover type and spatial resolution for modeling plot level forest attributes using multispectral airborne LiDAR data. ISPRS J. Photogramm. Remote Sens. 169, 152–165. https://doi.org/10.1016/j.isprsjprs.2020.09.001.
Yoon, T.K., Park, C.-W., Lee, S.J., Ko, S., Kim, K.N., Son, Y., Lee, K.H., Oh, S., Lee, W.-K., Son, Y., 2013. Allometric equations for estimating the aboveground volume of five common urban street tree species in Daegu. Korea. Urban For. Urban Green. 12 (3), 344–349. https://doi.org/10.1016/j.ufug.2013.03.006.
Zhang, L., Grift, T.E., 2012. A monocular vision-based diameter sensor for Miscanthus giganteus. Biosyst. Eng. 111 (3), 298–304. https://doi.org/10.1016/j.biosystemseng.2011.12.007.
Zhang, Z., 2000. A flexible new technique for camera calibration. IEEE Trans. Pattern Anal. Mach. Intell. 22, 1330–1334. https://doi.org/10.1109/34.888718.